Supplementary Material: Explanation of angle of linear polarization estimator error

Joaquin Rodriguez, Lew-Fock-Chong Lew-Yan-Voon, Renato Martins, and Olivier Morel
ImViA, Université de Bourgogne, Le Creusot, France

This is supplementary material of our RAL/IROS 2022 submission entitled **"A practical calibration method for RGB micro-grid polarimetric cameras"**. This document includes additional demonstrations and experiments that might be of interest for the readers.

Appendix A: Sine-like shape of the AoLP estimator error

In this appendix, we demonstrate why the error of the AoLP estimator has a sine-like shape. This demonstration is auxiliary to the submitted paper and the explanation was not included in the main paper due to space restrictions. The shape shown in Fig. 1 is a plot of error in the circular average of the angle of linear polarization. The estimated angle is calculated from the intensity measurements of a 50×50 region around the center of the sensor with a 16mm lens. For each AoLP, ten images of a uniform, linearly polarized light are captured and averaged to reduce the influence of the noise in the estimations.

I. Demonstration

When a pixel and its polarization filter are not ideal, the relationship between the Stokes vector and its measured intensity is given by Eq. (6) in the main paper:

$$I_i = T_i \begin{bmatrix} \frac{1}{P_i} & \cos(2\theta_i) & \sin(2\theta_i) \end{bmatrix} \begin{bmatrix} S_0 \\ S_1 \\ S_2 \end{bmatrix}, \quad (1)$$

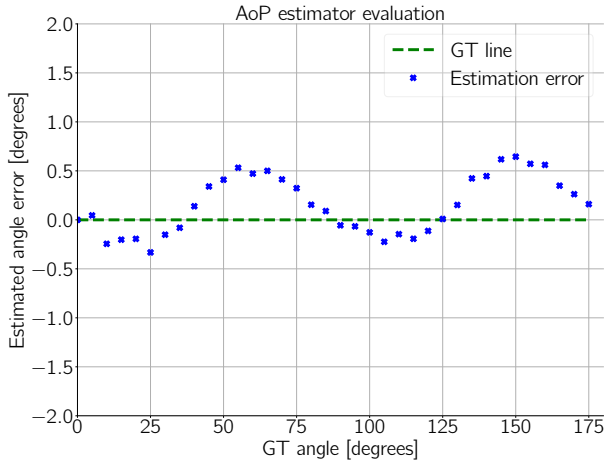

Fig. 1. AoLP estimator error plot.

where I_i is the measured pixel intensity, T_i is the pixel gain, P_i is a factor that models the non-ideality of the pixel micro-filter, and θ_i is the micro-filter orientation, for $i = \{0°, 45°, 90°, 135°\}$.

To demonstrate the error equation in the estimated AoLP, we compute the error in the measured Stokes components when the pixels are considered ideal.

$$\begin{aligned} \hat{S}_1 &= I_0 - I_{90} \\ \hat{S}_2 &= I_{45} - I_{135} \end{aligned} \quad (2)$$

Considering the pixel model of Eq. (1), and assuming that the micro-filter with orientation i has an error $\Delta\theta_i$ with respect to its ideal orientation, we obtain:

$$\hat{S}_1 = \left[T_0 \begin{bmatrix} \frac{1}{P_0} & \cos(2\Delta\theta_0) & \sin(2\Delta\theta_0) \end{bmatrix} - T_{90} \begin{bmatrix} \frac{1}{P_{90}} & \cos(\pi + 2\Delta\theta_{90}) & \sin(\pi + 2\Delta\theta_{90}) \end{bmatrix} \right] \begin{bmatrix} S_0 \\ S_1 \\ S_2 \end{bmatrix} \quad (3)$$

Using the sine and cosine properties, and grouping terms gives:

$$\hat{S}_1 = \begin{bmatrix} A & B & C \end{bmatrix} \begin{bmatrix} S_0 \\ S_1 \\ S_2 \end{bmatrix}, \quad (4)$$

with

$$A = \frac{T_0}{P_0} - \frac{T_{90}}{P_{90}}$$

$$B = T_0 \cos(2\Delta\theta_0) + T_{90} \cos(2\Delta\theta_{90})$$

$$C = T_0 \sin(2\Delta\theta_0) + T_{90} \sin(2\Delta\theta_{90})$$

Since the angle error can be considered close to zero, then the corresponding Taylor expansions up to order two can be used to replace the sine and cosine functions. Moreover, by doing the matricial multiplication we obtain:

$$\hat{S}_1 = AS_0 + \left[T_0 + T_{90} - 2T_0\Delta\theta_0^2 - 2T_{90}\Delta\theta_{90}^2\right] S_1 + \left[2T_0\Delta\theta_0 + 2T_{90}\Delta\theta_{90}\right] S_2. \quad (5)$$

If the angle errors are between $[-10°, 10°]$, the corresponding range in radians is $[-0.1745, 0.1745]$. Thus, if we square this range, we obtain a range of values $[0, 0.03]$. The orientation errors due to manufacturing problems have values

less than $10°$, therefore, the second order variables can be ignored, i.e.:

$$\hat{S}_1 = AS_0 + G^{'}S_1 + K_1S_2. \tag{6}$$

with:

$$G^{'} = T_0 + T_{90}$$

$$K_1 = 2T_0\Delta\theta_0 + 2T_{90}\Delta\theta_{90}.$$

Similarly, $\hat{S}_2$ can be obtained as a function of the Stokes components.

$$\hat{S}_2 = DS_0 - K_2S_1 + G^{''}S_2. \tag{7}$$

where:

$$D = \frac{T_{45}}{P_{45}} - \frac{T_{135}}{P_{135}}$$

$$G^{''} = T_{45} + T_{135}$$

$$K_2 = 2T_{45}\Delta\theta_{45} + 2T_{135}\Delta\theta_{135}.$$

It follows that the estimated AoLP $\hat{\alpha}$ is equal to:

$$\hat{\alpha} = \frac{1}{2}\arctan\left(\frac{\hat{S}_2}{\hat{S}_1}\right) = \frac{1}{2}\arctan\left(\frac{DS_0 - K_2S_1 + G^{''}S_2}{AS_0 + G^{'}S_1 + K_1S_2}\right) \tag{8}$$

Remembering that $S_1 = S_0\rho\cos(2\alpha)$, and $S_2 = S_0\rho\sin(2\alpha)$, where ρ is the degree of linear polarization, and α is the angle of linear polarization of the incoming light, Eq. (8) becomes:

$$\hat{\alpha} = \frac{1}{2}\arctan\left(\frac{D - K_2\rho\cos(2\alpha) + G^{''}\rho\sin(2\alpha)}{A + G^{'}\rho\cos(2\alpha) + K_1\rho\sin(2\alpha)}\right) \tag{9}$$

This equation converges to the true AoLP α if the pixels and the filters are ideal, i.e., $P_i = 1$, $T_i = 0.5$, and $\Delta\theta_i = 0$, for $i = \{0, 45, 90, 135\}$. In a real case, slight deviations from these values will appear. The sources of these deviations are the manufacturing process of the sensor, and the lens added to the camera. As mentioned in the main paper, considering a small region around the center of the sensor reduces the deviations caused by the lens.

Analyzing this equation, it is possible to conclude that:

- The deviations in the pixel parameters will make the other Stokes parameters to influence the AoLP measurement.
- The deviations in the orientations of the micro-polarizers, denoted by $\Delta\theta_i$, for $i = \{0, 45, 90, 135\}$ will introduce an error based on the value of the complementary Stokes parameter (for the measurement of S_1, a deviation in the orientation of the micro-polarizers will introduce an error based on the value of S_2, and an error based on S_1 in the measurement of S_2).
- For measurements of the same light at different AoLP, the deviations in the non-ideality factor P_i and the gain T_i will produce a constant shift in both, numerator and denominator, of Eq. (9).
- The values of K_1 and K_2 should be close to zero, and this can happen in two situations: either the pixel parameters are almost ideal and therefore the orientation errors are almost zero, or the pixels orientation error are almost the same, but in opposite directions. The second case can be understood by looking at the definitions of these variables. For instance, $K_1 = 2T_0\Delta\theta_0 + 2T_{90}\Delta\theta_{90}$, where T_0 and T_{90} are positive numbers, and in general, they are close to 0.5. Therefore, if $\Delta\theta_0 \simeq -\Delta\theta_{90}$, then K_1 will have a very tiny value. Similarly, K_2 will be almost zero when $\Delta\theta_{45} \simeq -\Delta\theta_{135}$. Finally, it can be seen that the errors in the orientations can be compensated if they are in opposite directions.

In all the cases, the errors will produce sine-like functions, since they will change the ratio of the sine to the cosine functions. Nevertheless, the effect of each parameter to the final shape of the error is different. The error in the orientations can change only the minimum and maximum values in the estimation error function, and the factors T_i and P_i can create sine shaped error functions and additionally change the position of its extreme values.

To test this formula, the error function has been computed for two set of samples from two different lenses. The samples to which the functions are fitted have been captured using the RGB polarization camera with the following lenses:

- Lens 1: Fuji-film HF16XA-5M - F1.6/16mm
- Lens 2: Fuji-film HF8XA-5M - F1.6/8mm

Lens 1 is the one used in the experiments in the main paper. Additionally, both lenses have been correctly focused on the light source used, and their F-number have been set to 3, which is higher than 2.8. This configuration have been chosen to comply with the recommendations given by [2].

To run this experiment, the AoLP estimator as described in the main paper has been implemented. Then, with a uniform unpolarized light source and a rotative linear polarization filter, a linearly polarized light is generated. The position of the filter is changed progressively in the range $[0°, 180°]$, with a step of $5°$. The reference angle of linear polarization of each sample have been measured from the rotative mount of the linear filter. Additionally, the AoLP is estimated with the implemented algorithm for each of these samples. Finally, the error between the reference value and the estimation is computed and plotted in Figs. 2 and 3.

By using a least-squares optimizer, the pixel parameters have been found for each set of samples taken with these lenses, and the results are shown in Tab. I. For creating this data, the degree of linear polarization was supposed to be $\rho = 0.97$.

As shown in Figs. 2 and 3, taking the measurements of the AoLP from the center pixels and doing their circular average, produces an estimation of the true AoLP with a maximum error of $0.65°$. This upper limit is valid for both lenses.

Tab. I shows all the pixel parameters obtained by least-squares optimization of Eq. (9) with the real data. From

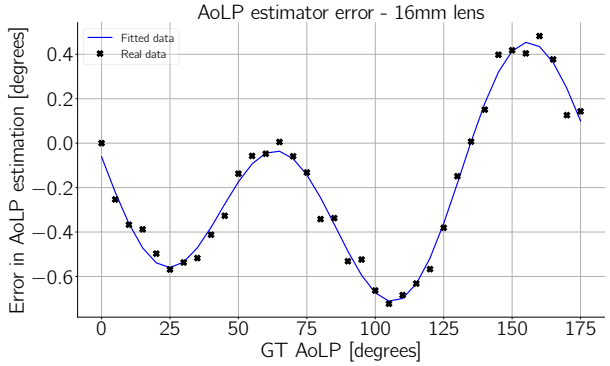

Fig. 2. Error in the AoLP and curve fitted of Eq. (9) for the lens 3

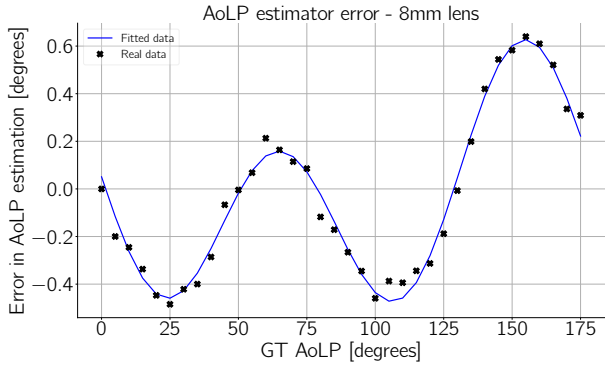

Fig. 3. Error in the AoLP and curve fitted of Eq. (9) for the lens 1

this table it is possible to confirm the effective pixel values are not far away from the ideal ones. Particularly, the maximum orientation error is $\Delta\theta_0 = 1.47°$. Nonetheless, as explained in the previous section, this error is compensated by the complementary pixel orientation which is, in this case, $\Delta\theta_{90} = -1.32°$. Additionally, the values exposed in this table show that the two lenses influence the pixel parameters. Indeed, the figures have similar shapes, but the corresponding maximum values are not the same, and they are located at different positions. This is because the corresponding pixel parameters have changed for each case. It is important to highlight that the estimation error in the AoLP is limited, and small (less than $0.65°$), confirming that the initial assumption of taking central pixels produces good estimates.

Lens model	Parameter	$i = \{0, 45, 90, 135\}$
T_i	Lens 1	$[0.53, 0.48, 0.49, 0.51]$
	Lens 2	$[0.525, 0.542, 0.548, 0.499]$
P_i	Lens 1	$[1.04, 0.88, 0.97, 0.95]$
	Lens 2	$[1.009, 0.992, 1.067, 0.922]$
$\Delta\theta_i$	Lens 1	$[1.47, -1.07, -1.32, 1.54]$
	Lens 2	$[0.109, 0.114, -0.192, 0.092]$

TABLE I

PARAMETERS OBTAINED BY NON-LINEAR OPTIMIZATION FOR EQ. (9).

APPENDIX B: APPLICATIONS TESTED WITH AND WITHOUT CALIBRATION

Since it is important to show the benefits of calibrating the RGB polarization camera in practical robot perception tasks, we have selected two testing algorithms for 3D geometry estimation. One for indoor and more suitable for small scale objects (shape-from-polarization), and one data-driven depth estimation approach from polarization images adapted to outdoor scenes. These algorithms are:

- *"Linear depth estimation from an uncalibrated, monocular polarisation image", ECCV, 2016* [3]: This paper proposes a shape-from-polarization algorithm with a linearization method for depth estimation, without any knowledge of the position of the light source. It is a geometric model-based approach, i.e., it does not use machine learning training phase for arriving to the results. We used the publicly available implementation in MatLab from the authors.
- *"P2D: a self-supervised method for depth estimation from polarimetry", ICPR 2020* [1]: This paper proposes a deep learning method for monocular disparity estimation, using monochrome polarization images. This network has been implemented considering the features given by the polarization state of the light. The code (in Python and PyTorch) and pre-trained model weights have been kindly provided by the authors of the paper upon our request.

The first experiment was the 3D reconstruction of a metallic, polished, parabolic object. This object has been placed at the interior of a dome, that provides a uniform, unpolarized, red light. The image has been captured with the camera that contains the Sony Polarsens sensor IMX250MYR, and a lens Fujinon HF8XA-5M. The object has been captured 1000 times, and the images have been averaged to reduce the influence of the noise. The camera has been calibrated, and then the intensities in the average image have been corrected with it. The reconstructed surfaces with and without calibration are shown in Fig. 5.

The areas of interest in this figure are highlighted with a green rectangle in the corresponding images. The corresponding images with the camera uncalibrated and calibrated are shown in the columns (c) and (d). In the reconstruction plots, we can notice two discontinuities. Since the surface is the result of an integration, the error in the normal's estimation will produce that the closing points, i.e., the region where the end joins the beginning of the surface, will not match. The error in the normal vectors is linked to the error in the estimation of AoLP and the DoLP (due to the pixel's parameters dispersion). These reconstruction artifacts have been reduced after calibration, with only one discontinuity in the surface with a reduced amplitude. It is important to mention that the same input images have been used for the two reconstructed surfaces. The uncalibrated reconstruction is done by using the raw image from the camera (after average), and the calibrated surface is obtained after correcting the measurements of the raw image.

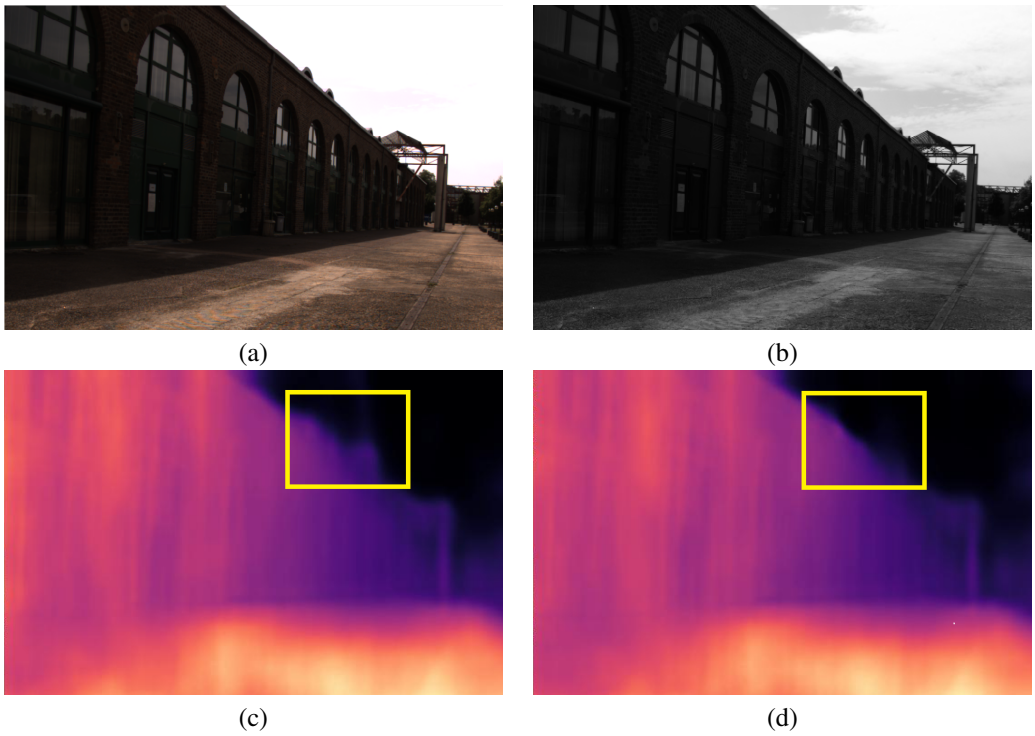

Fig. 4. Monocular disparity application example (hotter colors indicate larger disparity, i.e., smaller depth values). (a) Original color image. (b) Total intensity image (c) Disparity computed with the uncalibrated intensities. (d) Disparities computed with the calibrated intensities.

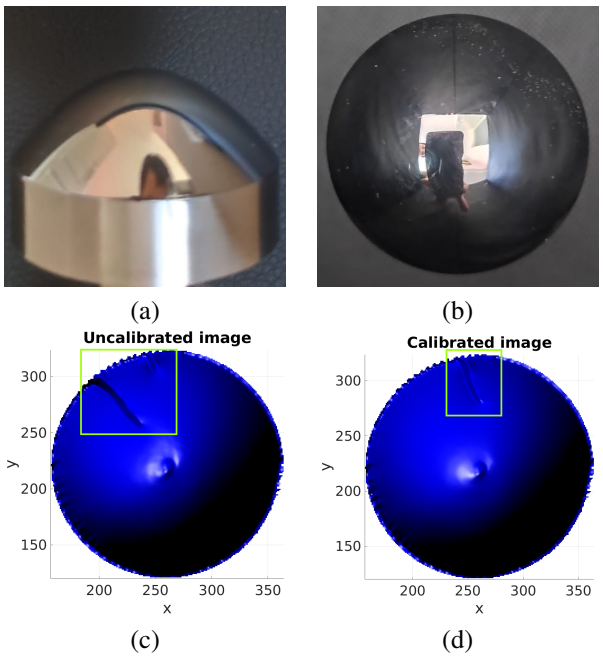

Fig. 5. 3D reconstruction application result. (a) Original piece - front view. (b) Original piece - top view. (c) 3D reconstruction top view of the piece with the uncalibrated camera. (d) 3D reconstruction top view of the piece with the calibrated camera.

The second application corresponds to a monocular disparity estimation technique using a deep neural network. The results before and after calibration are shown in Fig. 4. Again, some areas of interest are highlighted in yellow. Since the network was trained with monochrome polarization images, the total intensity per polarization channel have been computed and given to the network to produce the estimation.

In this case, we can notice that after calibration the roof region is improved. In the uncalibrated scenario, the network predicts a disparity that ascends towards the sky, and when the image is calibrated, the disparity of this region evolves following the border of the roof. There are two considerations that might explain this behavior: i) The sky is polarized, so the features given by it are very distinctive from the building. ii) Neural networks base their predictions per pixel considering its value and the ones of the neighbors pixels. An uncalibrated setup will estimate wrong polarization parameters due to the dispersion in the pixel parameters and due to the lens. Particularly, as explained in the paper, the lens will produce a change in the polarization state depending on the point of incidence of the light at the lens surface. This change will create a gradient in the values different to the one present in the real scene. By doing the calibration, we reduce the lens effect, and therefore making the depth estimation between objects closer to the one in the real-scene.

REFERENCES

[1] Marc Blanchon, Désiré Sidibé, Olivier Morel, Ralph Seulin, Daniel Braun, and Fabrice Meriaudeau. P2D: a self-supervised method for depth estimation from polarimetry. In International Conference on Pattern Recognition, 2020.

[2] Connor Lane, David Rode, and Thomas Roesgen. Calibration of a polarization image sensor andinvestigation of influencing factors. Applied Optics, 61, 10 2021.

[3] William A. P. Smith, Ravi Ramamoorthi, and Silvia Tozza. Linear depth estimation from an uncalibrated, monocular polarisation image. In Bastian Leibe, Jiri Matas, Nicu Sebe, and Max Welling, editors, Computer Vision – ECCV 2016, 2016.